

Supporting Information for

Hollow PdCuMoNiCo high-entropy alloy as an efficient bi-functional electrocatalyst for oxygen reduction and formic acid oxidation

Xifeng Zuo,^{†a} Riqing Yan,^{†a} Linjie Zhao,^a Yongde Long,^a Lei Shi,^a Qingqing Cheng,^{*b}
Dong Liu,^{*a} Chuangang Hu^{*a}

Supplementary Methods

Chemicals. Copper chloride (CuCl_2 , $\geq 98\%$), cobalt chloride (CoCl_2 , $\geq 99.7\%$), Palladium chloride (PdCl_2 , 59-60%), nickel chloride hexahydrate ($\text{NiCl}_2 \cdot 6\text{H}_2\text{O}$, $\geq 98\%$), ethylene glycol ($\text{C}_2\text{H}_6\text{O}_2$, $\geq 99\%$) and perchloric acid (HClO_4 , 59-60%) were purchased from Aladdin. Sodium molybdate dehydrate ($\text{Na}_2\text{MoO}_4 \cdot 2\text{H}_2\text{O}$, $\geq 99.0\%$) was purchased from General-Reagent. Formic acid (98%) was purchased from J&K. Isopropyl alcohol ($\text{C}_3\text{H}_8\text{O}$, $\geq 99.5\%$), and potassium hydroxide (KOH, 99.99%) was purchased from Macklin. L-Glutamic acid ($\geq 99.5\%$) was purchased from Innochem Technology Co., Ltd. (Shanghai, China). Methanol (CH_3OH , $\geq 99.5\%$) was purchased from Damao Chemical Reagent Factory (Tianjin, China). All chemicals were used without further purification. The aqueous solution used in the experiment was ultrapure water with a resistivity of 18.25 $\text{M}\Omega \text{ cm}$.

Characterization. Scanning electron microscopy (SEM) was performed using Ziess Supra55. Transmission electron microscopy (TEM), high-resolution TEM (HR-TEM), high-resolution high-angle annular dark-field scanning TEM (HAADF-STEM), energy-dispersive X-ray spectroscopy (EDS), and elemental mappings were acquired on JEM-2010 (HR) operating at 200 kV. X-ray diffraction (XRD) patterns of the samples were recorded on a Bruker D2 Phaser diffractometer with $\text{Cu K}\alpha$ radiation ($\lambda = 1.54184 \text{ \AA}$). X-ray photoelectron spectra (XPS) were collected on a Thermo

Scientific K-Alpha, using Al K α X-ray radiation (1486.6 eV) for excitation. Binding energies were corrected from charge effects by reference to the C1s peak of carbon at 284.6 eV. The inductively coupled plasma optical emission spectrometry (ICP-OES) analysis of samples was performed on Agilent ICP-OES 725 ES.

Synthesis of graphene oxide (GO). 3.0 g of graphite powder and 1.5 g of NaNO₃ were added to 70 mL of concentrated sulfuric acid and stirred in an ice-water bath. Then, 9.0 g of KMnO₄ was slowly added to the above solution under continuous stirring while the temperature was controlled below 20 °C during this process. Then the solution was heated to 35 °C and stirred for 1 h, followed by adding 15 mL of water, and the temperature was raised to 80 °C for 15 min. After cooling down to room temperature, 500 mL of deionized water and 15 mL of H₂O₂ (30%) were added. After standing for 2 h, the upper supernatant was removed, and the remaining solid was washed with 10% hydrochloric acid several times. Then the filter cake was dispersed in deionized water and centrifuged at 10,000 rpm to obtain the precipitate. Finally, the precipitate was dispersed in deionized water and dialyzed for two weeks to obtain GO.

Synthesis of oxidized carbon nanotubes (O-CNT). First, 2.0 g of carbon nanotube were calcined in air at 430 °C for 1 h, and then stirred in a mixture of sulfuric acid and nitric acid (3:1, volume ratio) at 60 °C for 3 h. After cooling to room temperature, the solid was obtained by centrifugation three times with dilute hydrochloric acid and deionized water, respectively. The solid was then dispersed in deionized water and dialyzed for one week. Finally, the O-CNT was obtained after vacuum freeze-drying.

Synthesis of PdCuMoNiCo nano-hollow spherical HEA on RGO₃-CNT (PdCuMoNiCo NHSs/RGO₃-CNT). Firstly, 25.6 mg of carbon support (GO: O-CNT = 3:1, mass ratio) was added to 30 mL of ethylene glycol and dispersed uniformly by ultrasonic for 1 h. Then, 50 mg of glutamic acid was added, followed by 1.50 mL of 6.7 mg mL⁻¹ PdCl₂, 0.190 mL of 40 mg mL⁻¹ CuCl₂, 0.184 mL of 40 mg mL⁻¹ CoCl₂, 0.337 mL of 40 mg mL⁻¹ NiCl₂·6H₂O, and 0.343 mL of 40 mg mL⁻¹ Na₂MoO₄·2H₂O. The above solution was continuously dispersed by ultrasonic for 1 h.

After that, 5 mL of ethylene glycol containing 8 wt. % potassium hydroxide was added to the solution under stirring to adjust the pH of the solution to alkaline. Then, the suspension was transferred into a 50 mL Teflon-lined stainless-steel autoclave followed by thermal treatment at 160 °C for 7 h. After cooling down to room temperature, the solid was obtained after filtration and washed with deionized water and ethanol for several times. Finally, PdCuMoNiCo NHSs/RGO₃-CNT was obtained after vacuum freeze-drying.

Electrochemical measurements. A three-electrode system was used for the electrochemical measurements. Catalyst (1.5 mg), isopropanol (495 μL), water (495 μL), and Nafion solution (5 wt. %, 10 μL) were added to a 2 mL centrifuge tube, and sonicated for 1 h to form a uniform ink. The electrocatalytic performance of the catalyst was evaluated by using a glassy carbon (GC) rotating ring-disk electrode (RRDE, 4 mm in diameter) as the working electrode on a CHI 760E electrochemical workstation (CH Instruments, Inc., Shanghai). The Ag/AgCl electrode and platinum wire were selected as the reference and counter electrodes, respectively. Before depositing the catalyst, the electrode was polished with Al₂O₃ powder and then thoroughly rinsed with deionized water three times. For the ORR measurement, to prepare the working electrode, 20 μL of catalyst ink was dropped onto the GC RRDE and then dried under ambient conditions. The ORR measurements were performed in an O₂-saturated 0.1 M HClO₄ solution at room temperature. The current-time curves were recorded at 0.5 V vs. RHE at a rotation speed of 1,600 rpm. The mass activity (MA) related kinetic current density for ORR was calculated according to (S1):

$$MA = j_k/M_{Pd} = j \times j_d / ((j_d - j) \times M_{Pd}) \quad (S1)$$

where j_k , j , j_d and M_{Pd} are the kinetic current, measured current, diffusion-limited current, and Pd loading, respectively.

The Koutecky-Levich (*K-L*) plots were obtained by linear fitting the reciprocal rotating speed versus reciprocal current density collected at 0.3 V, 0.4 V, 0.5 V, and 0.6 V, respectively. The electron transfer number involved in a typical ORR process

can be calculated from the slopes of K - L equation (S2) as follows:

$$1/j = 1/j_k + 1/j_d = 1/j_k + 1/(B\omega^{1/2})$$

$$B = 0.2nFA\nu^{-1/6}C_{O_2}(D_{O_2})^{2/3} \quad (S2)$$

where “ n ” is the number of electrons transferred, F is the Faraday constant (96485 C mol⁻¹), A is the surface area of the electrode, D_{O_2} is the diffusion coefficient of O₂, ν is the kinetic viscosity, and C_{O_2} is the concentration of O₂. The constant 0.2 is adopted when the rotating speed is in rpm.

The peroxide percentage (H₂O₂%) and “ n ” can be determined from RRDE measurements based on the disk current and ring current based on the equations (S3 and S4):

$$H_2O_2\% = 200 \times I_r / (I_d \times N + I_r) \quad (S3)$$

$$n = 4 \times N \times I_d / (I_d \times N + I_r) \quad (S4)$$

where the I_d and I_r are the disk current and ring current, respectively, N is the current collection efficiency of the Pt ring (0.424).

In the FAO test, 10 μ L of catalyst ink was covered on a GC RRDE (4 mm in diameter) to prepare the working electrode. For the electrocatalytic oxidation of formic acid, the CVs were recorded in Ar-saturated 0.1 M HClO₄ + 0.5 M HCOOH solution at room temperature from -0.3 to 1.0 V vs. Ag/AgCl at a sweep rate of 50 mV s⁻¹. The current-time curves were recorded at 0.5 V vs. RHE at a rotation speed of 1,600 rpm. The mass activity for FAO was calculated according to (S5):

$$MA = j/M_{Pd} \quad (S5)$$

where j and M_{Pd} are the measured current and mass of Pd loading on the electrode.

CO stripping test: The electrochemically active surface area (ECSA) was estimated by CO stripping test. The catalyst was firstly tested for CV in Ar-saturated 0.1 M HClO₄ solution from 0.0 to 1.3 V vs. RHE at a scan rate of 50 mV s⁻¹ at room temperature, and after the CV was stabilized, it was then adsorbing CO at 0.2 V vs. RHE for 400 seconds. The CO stripping CVs were collected at a scan rate of 20 mV s⁻¹

¹ in Ar-saturated 0.1 M HClO₄ solution in the range of 0.2 to 1.3 V vs. RHE. The ECSA was calculated from the charge involved in the CO adsorption processes via the following equation (S6):

$$\text{ECSA} = Q / (0.42 \times M) \quad (\text{S6})$$

where Q (mC) is the charge for the CO adsorption. 0.42 (mC cm⁻²) is the electrical charge associated with monolayer adsorption of CO on Pd. M is the mass of Pd coating on the electrode. The average values and related errors for both ECSA and mass activity were obtained from the results based on the measurement of more than 5 electrodes made of each sample.

Supplementary Figures and Tables

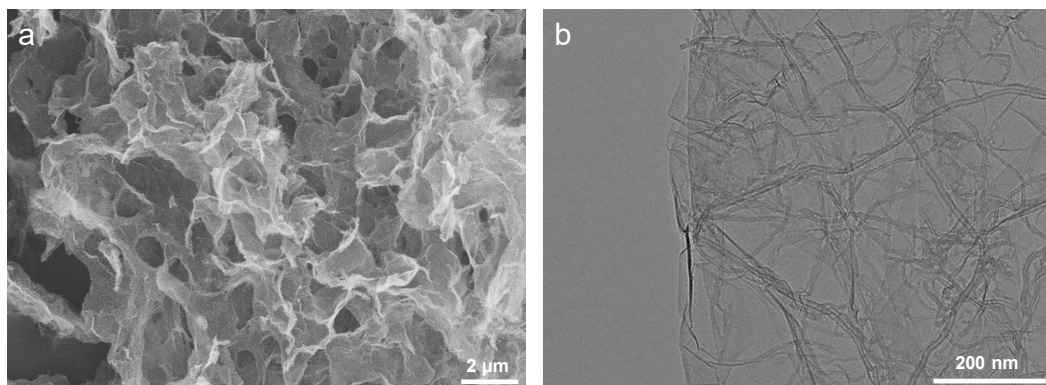


Figure S1. (a) SEM and (b) TEM images of the carbon hybrid derived from GO and O-CNT with the mass ratio of 3:1, which was prepared by the same method as the typical sample except for the absence of metal precursors.

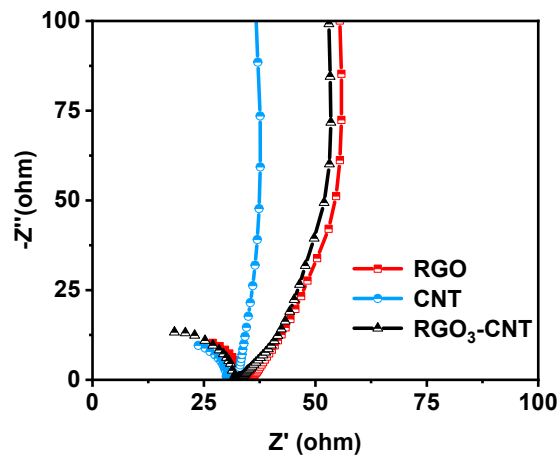


Figure S2. Electrochemical Impedance Spectroscopy (EIS) Nyquist plots of the carbon support derived from reduced graphene oxide (RGO), CNT, and RGO: CNT=3:1 (RGO₃-CNT), respectively. The charge transfer and ion diffusivity ability of RGO are enhanced by the CNT in RGO₃-CNT.

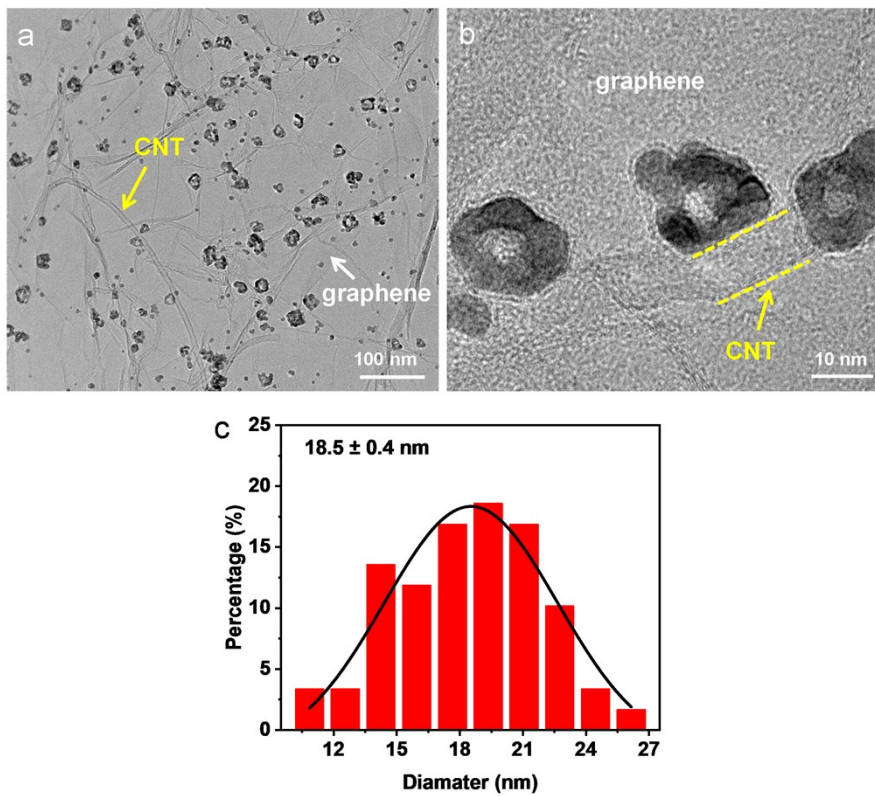


Figure S3. (a) TEM image, (b) HR-TEM image, and (c) the corresponding size distribution of the PdCuMoNiCo NHSs/RGO₃-CNT.

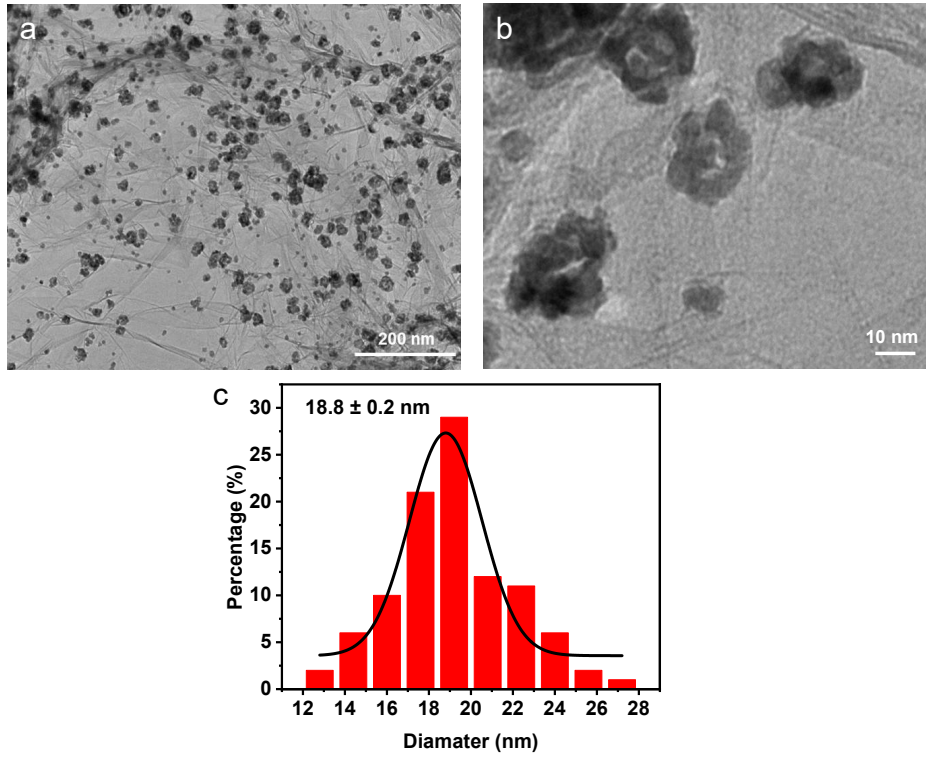


Figure S4. (a) TEM image, (b) HR-TEM image, and (c) the corresponding size distribution of the PdCuMoNiCo NHSs/RGO₃-CNT before acid treatment.

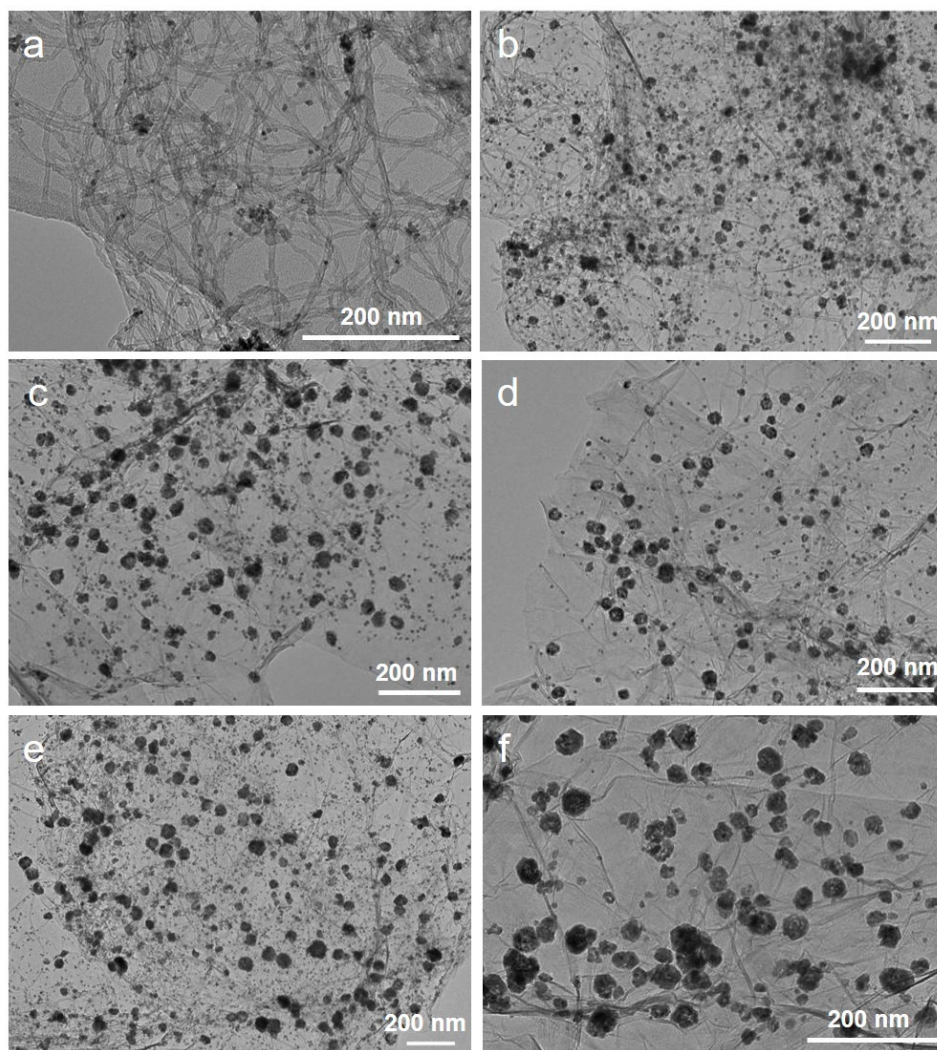


Figure S5. TEM images of the as-synthesized PdCuMoNiCo alloys on different carbon supports. The supports are (a) CNT, (b) RGO-CNT, (c) RGO₂-CNT, (d) RGO₄-CNT, (e) RGO₅-CNT, and (f) RGO, respectively.

The abundant functional groups on the surface of GO may provide favorable sites for anchoring the metal precursors, and the large surface area of 2D structure serves as a ideal support for the uniform dispersion of the individual hollow nanospheres.¹ Glutamic acid can coordinate with metal ions and further prevent particle agglomeration and regulate the morphology of HEA, a detailed discussion can be found in our previous report.^{1,2}

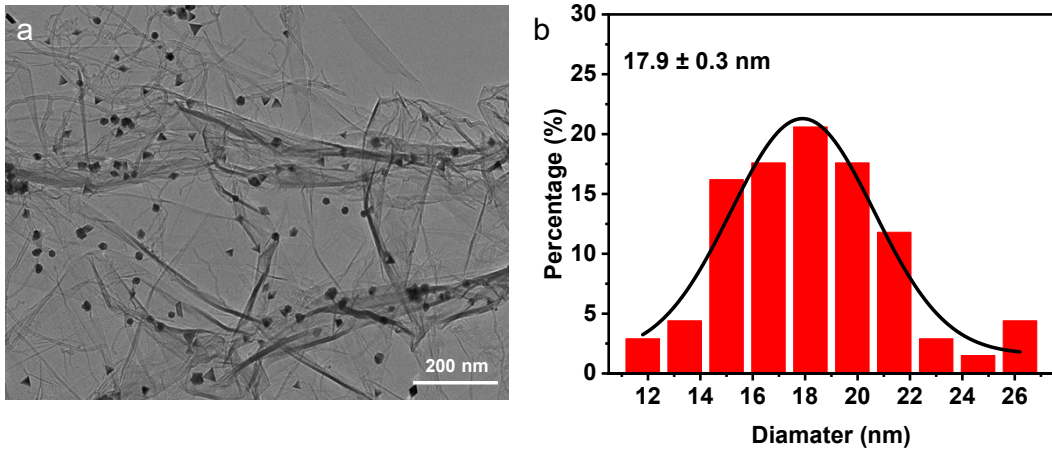


Figure S6. (a) TEM image and (b) the corresponding size distribution of the as-synthesized single Pd on RGO₃-CNT.

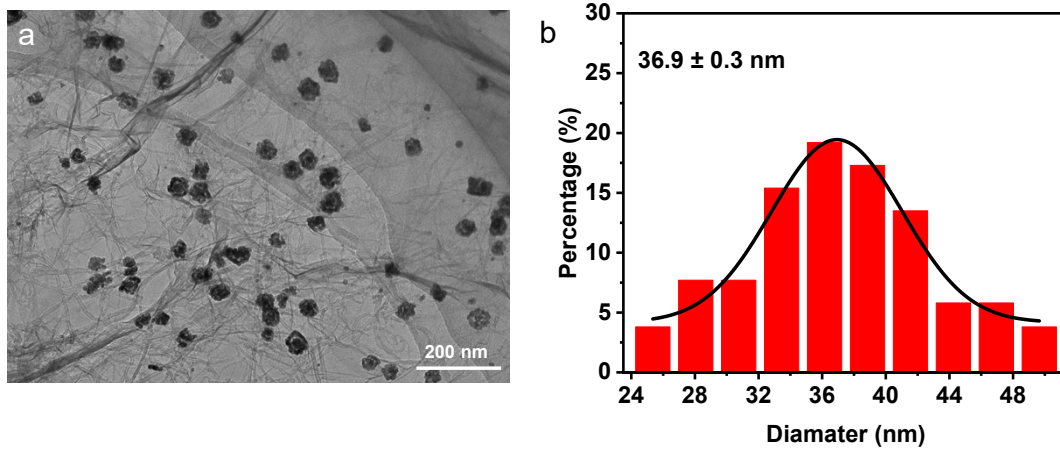


Figure S7. (a) TEM image and (b) the corresponding size distribution of the as-synthesized PdCu on RGO₃-CNT.

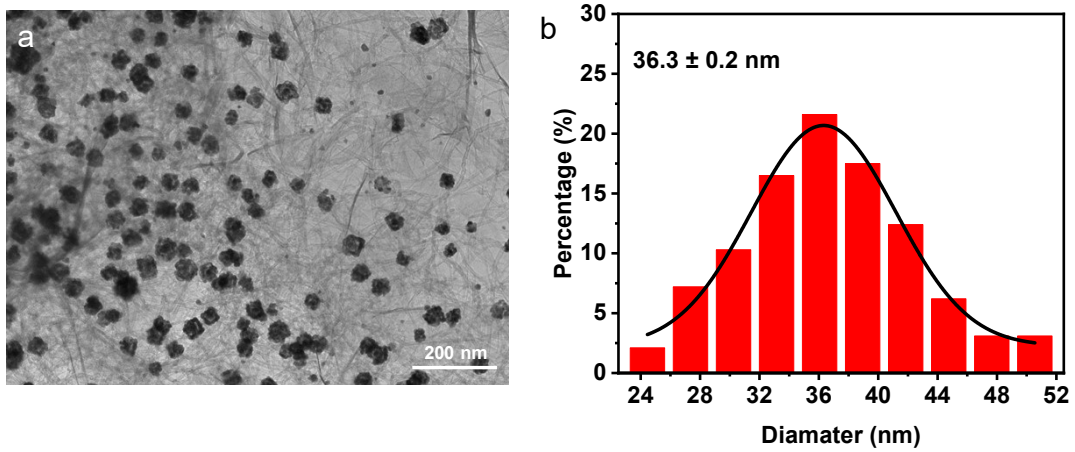


Figure S8. (a) TEM image and (b) the corresponding size distribution of the as-synthesized PdCuCo on RGO₃-CNT.

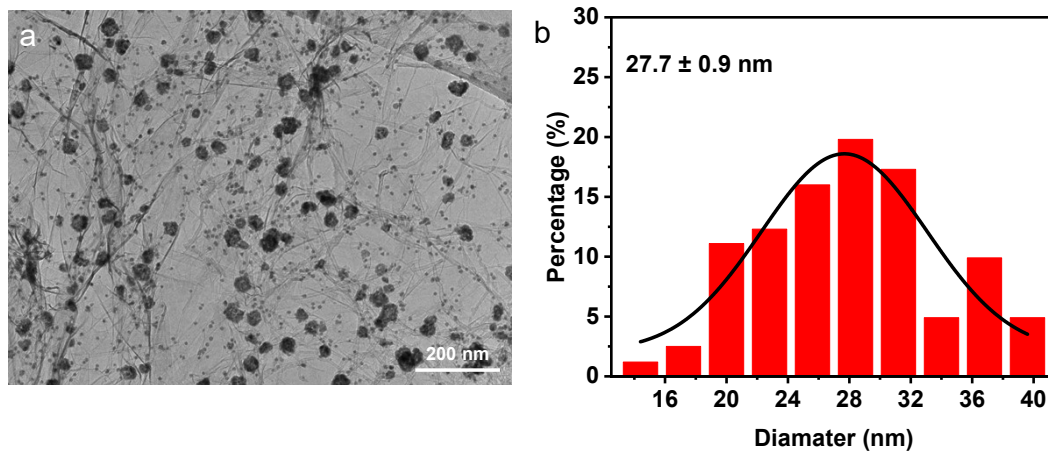


Figure S9. (a) TEM image and (b) the corresponding size distribution of the as-synthesized PdCuNiCo on RGO₃-CNT.

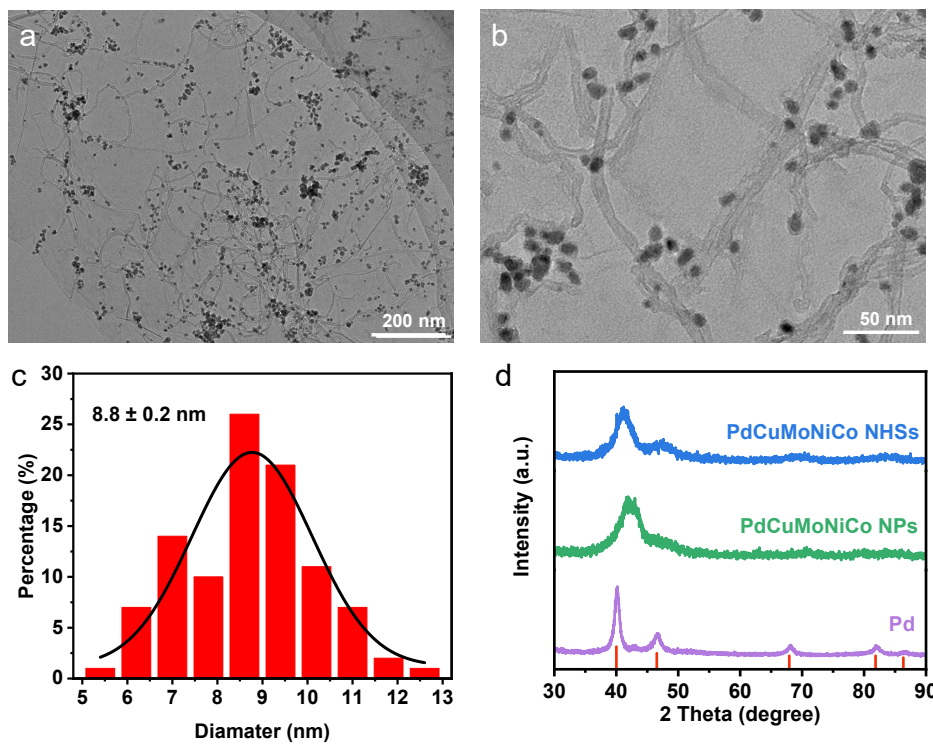


Figure S10. (a) TEM image, (b) HR-TEM image, and (c) the corresponding size distribution of the as-synthesized PdCuMoNiCo NPs/RGO₃-CNT. (d) XRD patterns of the PdCuMoNiCo NHSs/RGO₃-CNT, PdCuMoNiCo NPs/RGO₃-CNT, and single Pd on RGO₃-CNT, respectively.

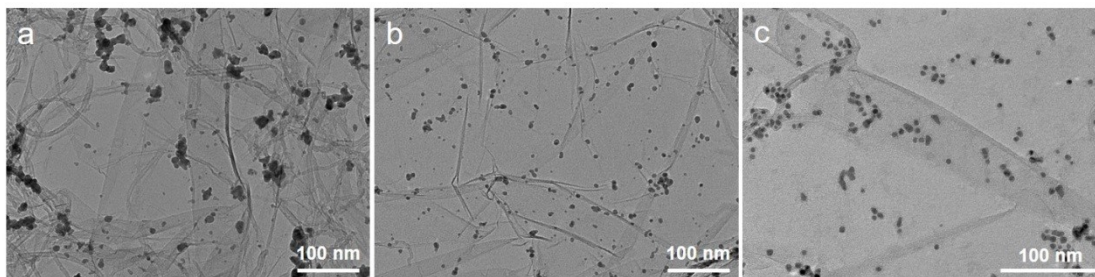


Figure S11. TEM images of the as-synthesized (a) PdCu nanoparticles (PdCu NPs), (b) PdCuCo nanoparticles (PdCuCo NPs), and (c) PdCuNiCo nanoparticles (PdCuNiCo NPs) on RGO₃-CNT. The preparation processes of PdCu NPs, PdCuCo NPs, and PdCuNiCo NPs were the same as that for the typical sample, except for the absence of glutamic acid and adding different metal precursors.

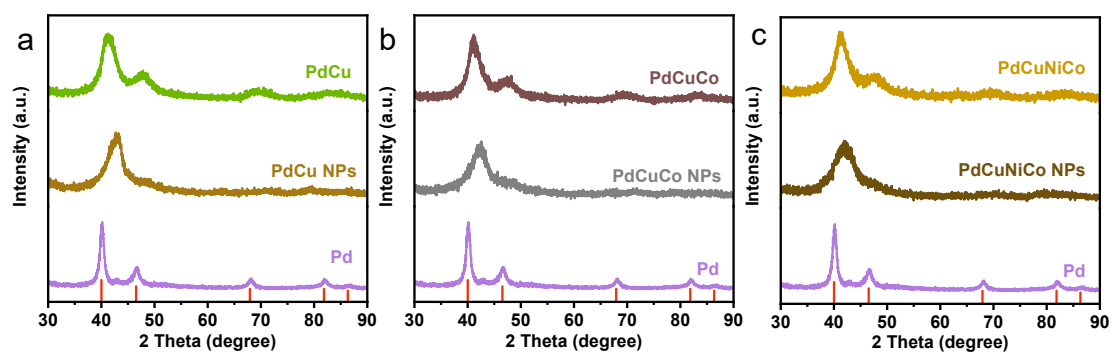


Figure S12. Comparison of XRD patterns of the as-synthesized (a) PdCu and PdCu NPs, (b) PdCuCo and PdCuCo NPs, (c) PdCuNiCo and PdCuNiCo NPs with single Pd on RGO₃-CNT, respectively.

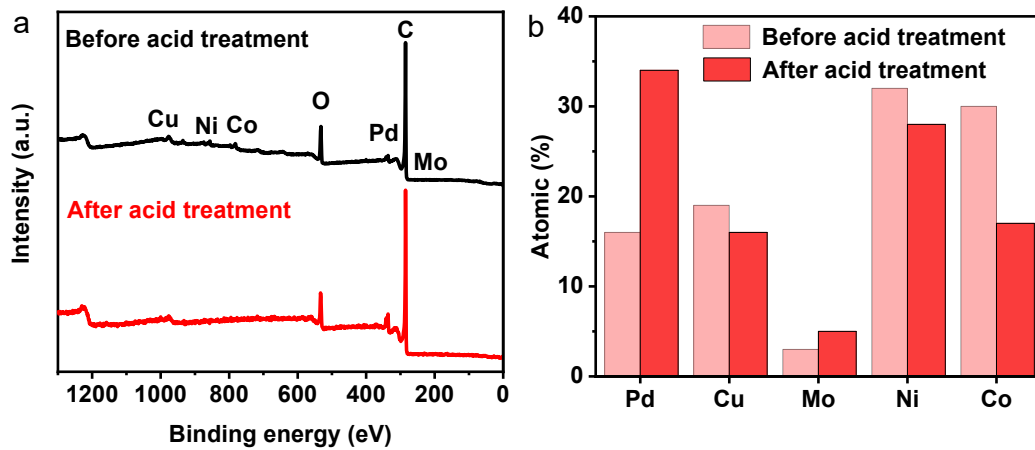


Figure S13. (a) XPS spectra of scan of the quinary PdCuMoNiCo NHSS/RGO₃-CNT before and after acid treatment. (b) The atomic ratios of different metals in PdCuMoNiCo NHSS/RGO₃-CNT before and after acid treatment were obtained from (a).

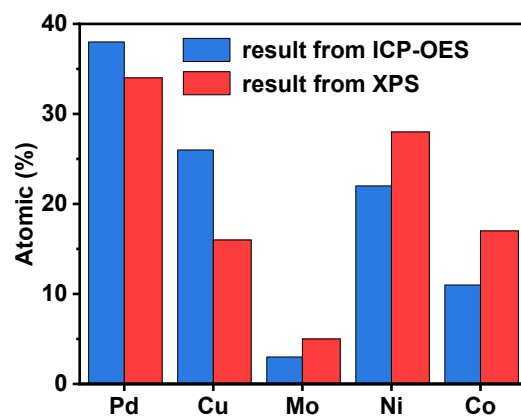


Figure S14. The atomic ratios of different metals in PdCuMoNiCo NHSs/RGO₃-CNT were obtained from XPS and ICP-OES, respectively.

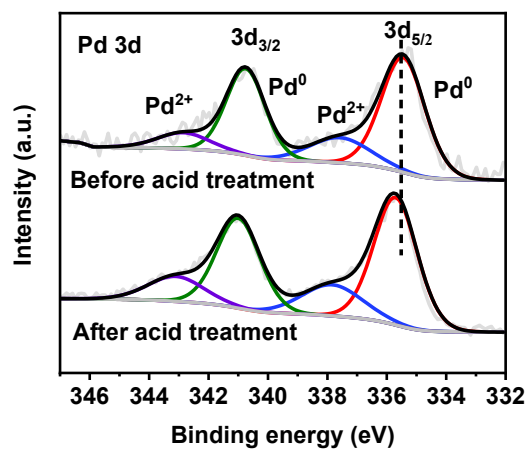


Figure S15. XPS spectra of Pd 3d for PdCuMoNiCo NHSs/RGO₃-CNT before and after acid treatment.

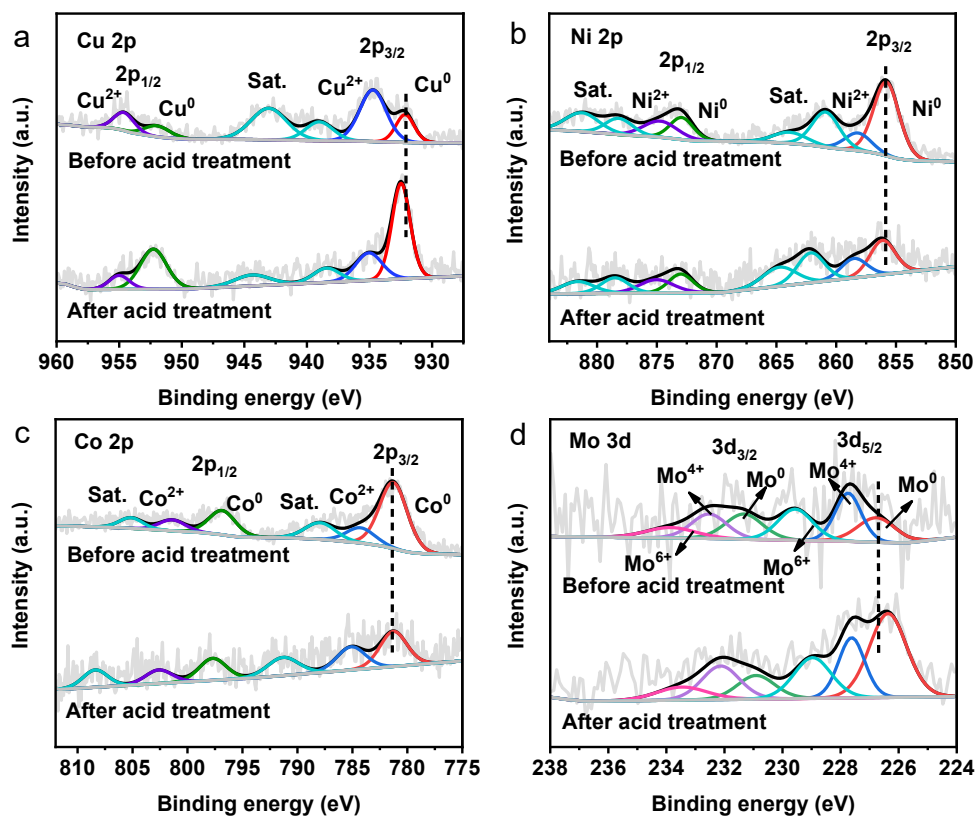


Figure S16. XPS spectra of (a) Cu 2p, (b) Ni 2p, (c) Co 2p, and (d) Mo 3d for PdCuMoNiCo NHSs/RGO₃-CNT before and after acid treatment.

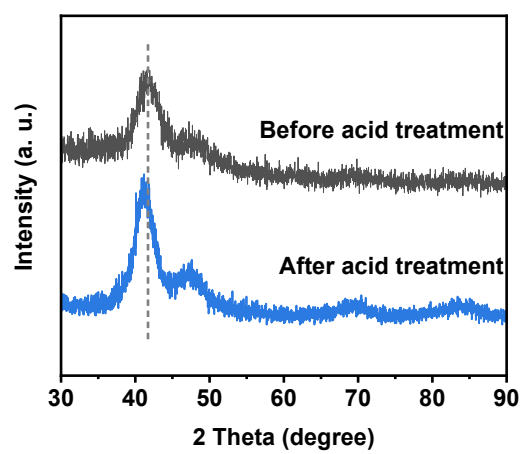


Figure S17. XRD patterns of PdCuMoNiCo NHSs/RGO₃-CNT before and after acid treatment.

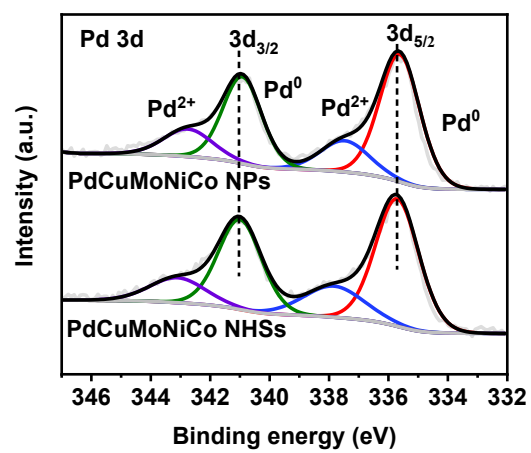


Figure S18. XPS spectra of Pd 3d for PdCuMoNiCo NHSs/RGO₃-CNT and PdCuMoNiCo NPs/RGO₃-CNT.

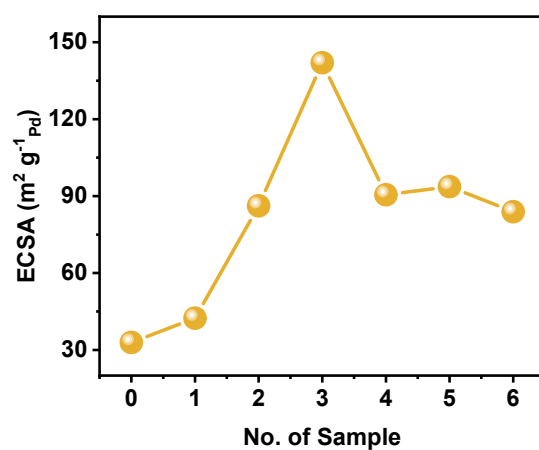


Figure S19. The ECSA of the as-synthesized PdCuMoNiCo alloys on different carbon supports. The supports represented by the numbers from 0 to 6 are CNT, RGO-CNT, RGO₂-CNT, RGO₃-CNT, RGO₄-CNT, RGO₅-CNT, and RGO, respectively.

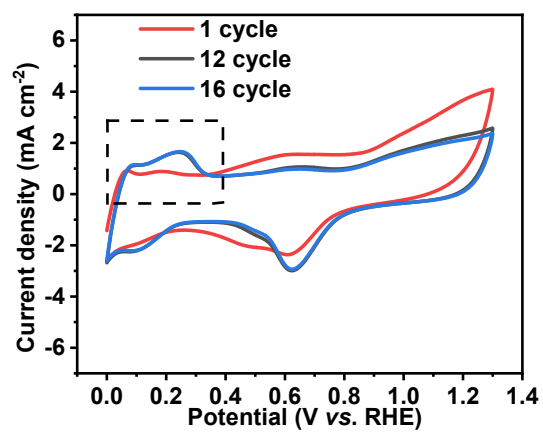


Figure S20. CV curves of the PdCuMoNiCo NHSs/RGO₃-CNT in 0.1 M HClO₄ solution until a steady state was obtained.

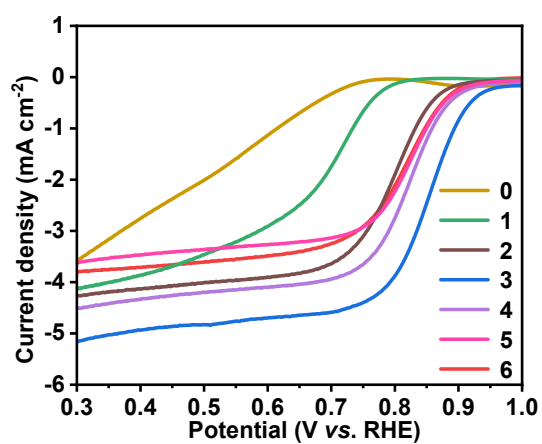


Figure S21. The comparison of ORR performance of the as-synthesized PdCuMoNiCo alloys on different carbon supports. The supports represented by the numbers from 0 to 6 are CNT, RGO-CNT, RGO₂-CNT, RGO₃-CNT, RGO₄-CNT, RGO₅-CNT, and RGO, respectively.

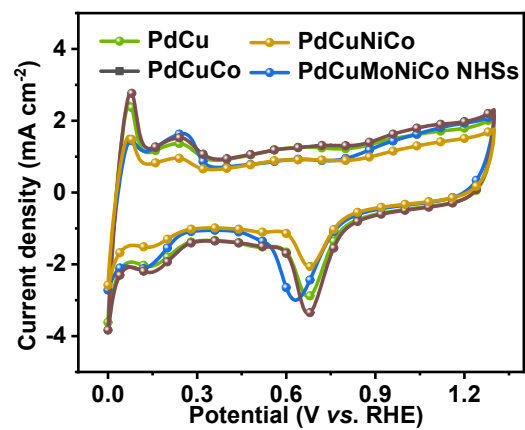


Figure S22. CV curves of the as-synthesized PdCu, PdCuCo, PdCuNiCo on RGO₃-CNT and PdCuMoNiCo NHSs/RGO₃-CNT in Ar-saturated 0.1 M HClO₄ solution at a scan rate of 50 mV s⁻¹.

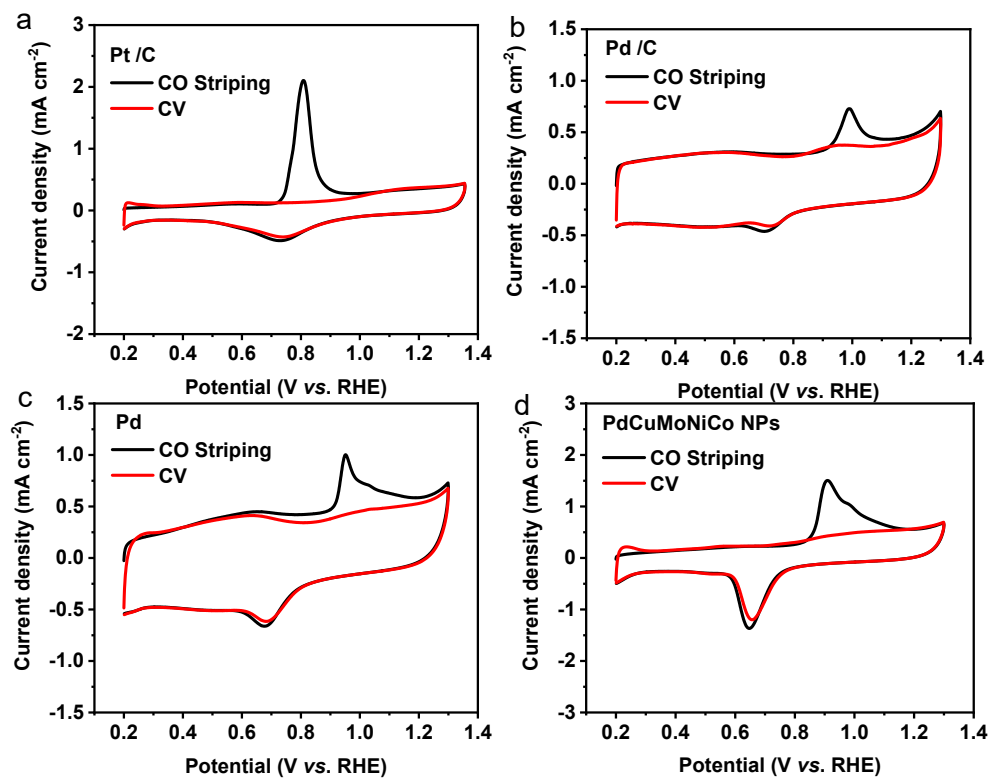


Figure S23. The CO-stripping curves of (a) commercial 20% Pt/C, (b) commercial 10% Pd/C, (c) the as-synthesized single Pd on RGO₃-CNT and (d) PdCuMoNiCo NPs/RGO₃-CNT.

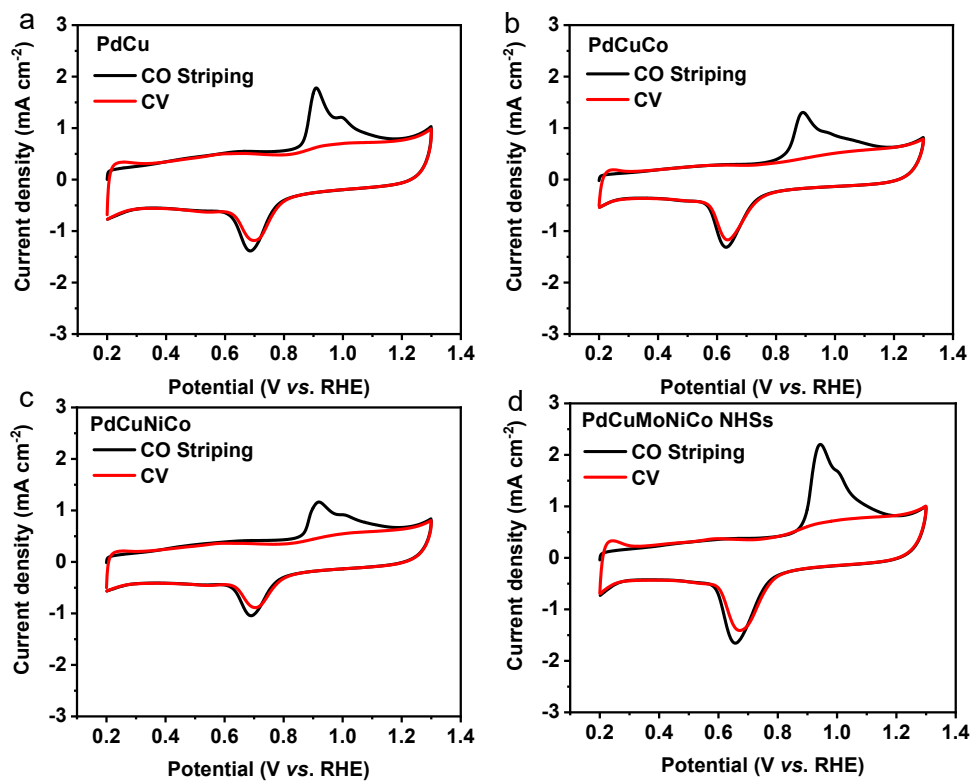


Figure S24. The CO-stripping curves of the as-synthesized (a) PdCu, (b) PdCuCo, (c) PdCuNiCo on RGO₃-CNT and (d) PdCuMoNiCo NHSs/RGO₃-CNT.

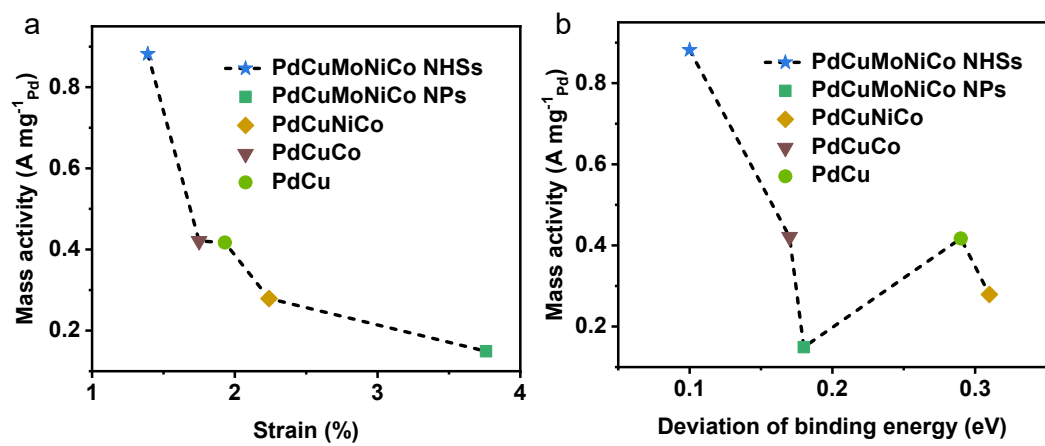


Figure S25. (a) The relationship between strain and MA of ORR. (b) The relationship between binding energy shift of Pd 3d XPS spectra and MA of ORR.

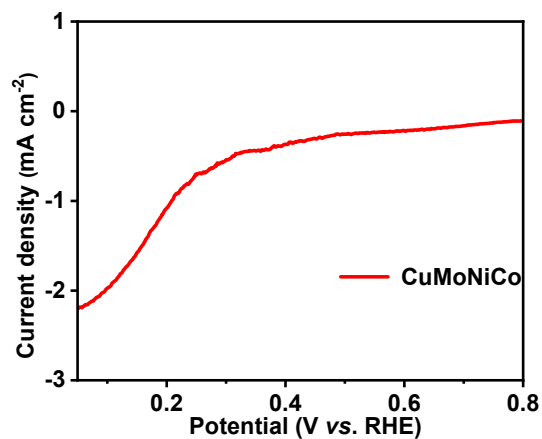


Figure S26. The ORR polarization curve of the as-synthesized CuMoNiCo on RGO₃-CNT in O₂-saturated 0.1 M HClO₄ solution at a scan rate of 5 mV s⁻¹ at a rotation rate of 1600 rpm. The preparation process of CuMoNiCo on RGO₃-CNT was the same as that for the typical sample except for the absence of PdCl₂ precursor.

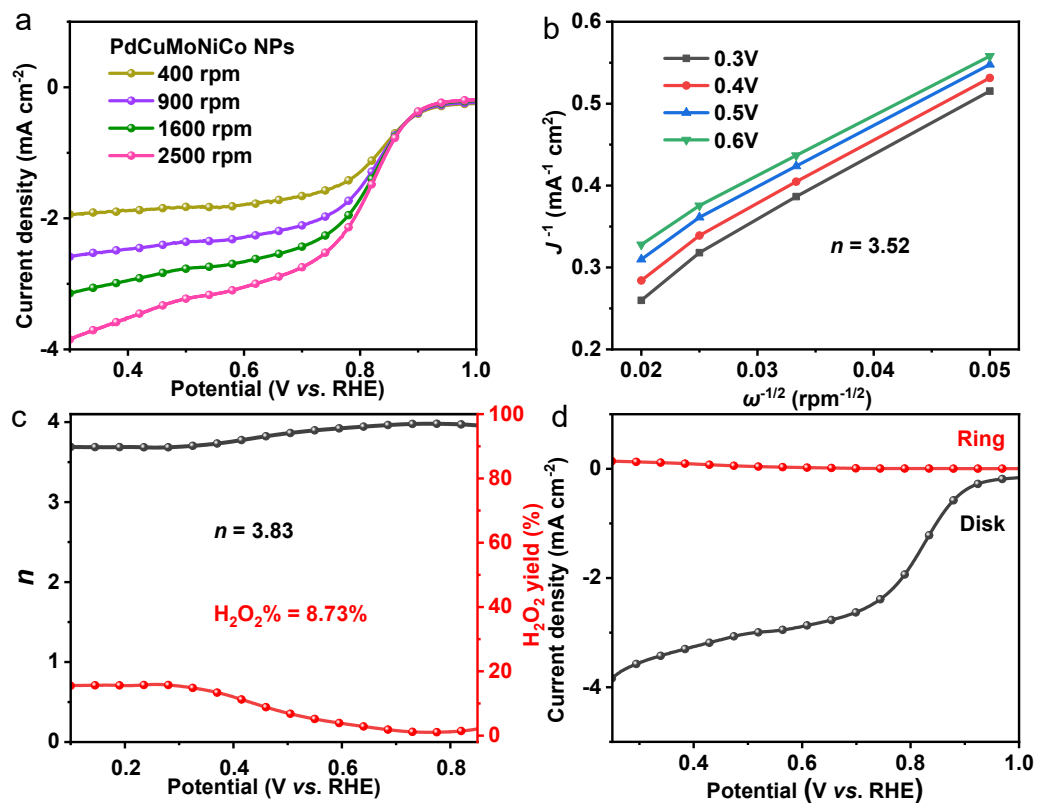


Figure S27. (a) The ORR polarization curves of PdCuMoNiCo NPs/RGO₃-CNT at different rotating rates. (b) The corresponding *K-L* plots at different potentials. (c) The electron transfer number and H₂O₂ yield of PdCuMoNiCo NPs/RGO₃-CNT. (d) The corresponding disk and ring current of PdCuMoNiCo NPs/RGO₃-CNT (the Pt ring electrode was maintained at 1.4 V vs. RHE).

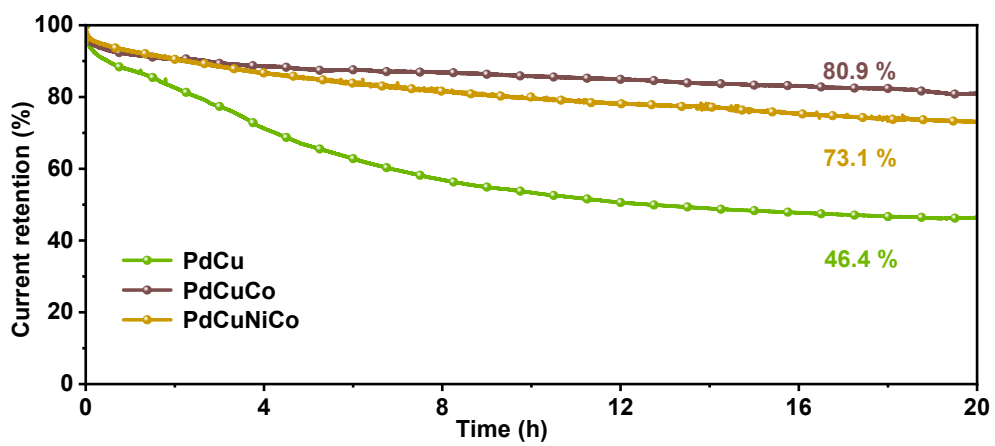


Figure S28. The current-time curves of the PdCu, PdCuCo, and PdCuNiCo on RGO₃-CNT for ORR at 0.5 V vs. RHE, respectively.

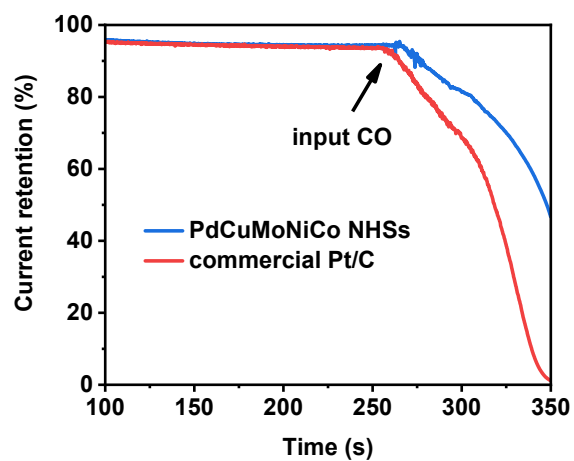


Figure S29. The CO tolerance of PdCuMoNiCo NHSs/RGO₃-CNT and commercial 20% Pt/C in O₂-saturated 0.1 M HClO₄ solution with the introduction of CO.

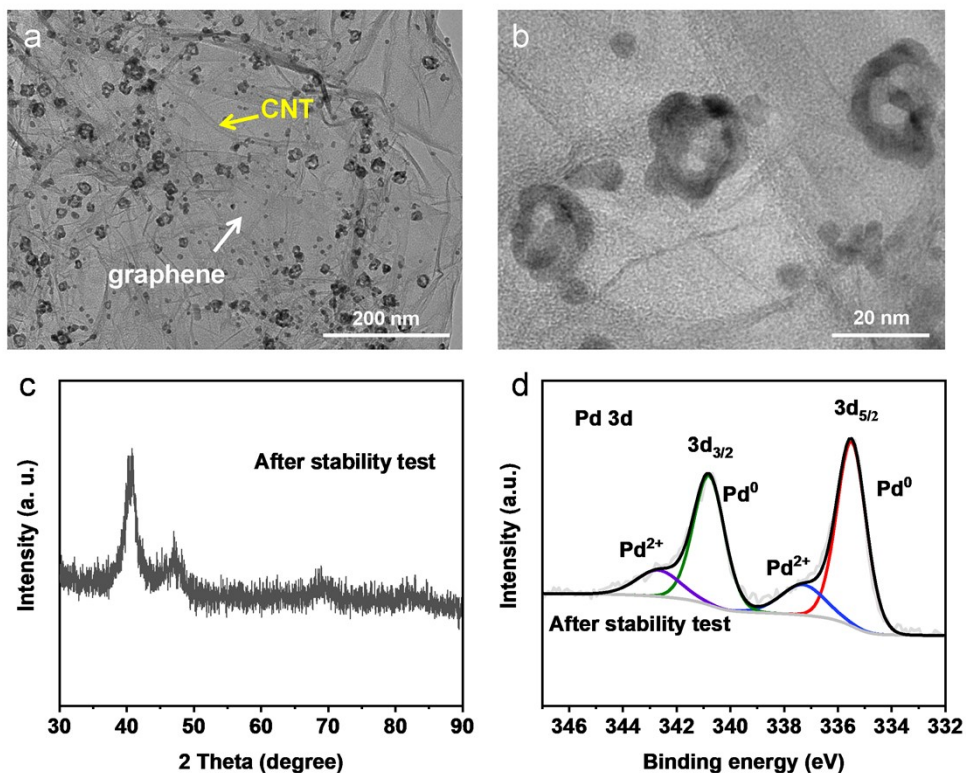


Figure S30. (a) TEM image, (b) HR-TEM image, (c) XRD pattern, and (d) High resolution of Pd 3d XPS spectrum of the PdCuMoNiCo NHSs/RGO₃-CNT after long-term durability test for ORR.

There was no obvious aggregation or structural change of the PdCuMoNiCo NHSs/RGO₃-CNT catalyst as shown by the TEM images (Figure S30a,b) and XRD pattern (Figure S30c) after the long-term durability test. The chemical state of Pd in PdCuMoNiCo NHSs/RGO₃-CNT was well maintained from XPS spectra before and after the durability test (Figure S30d).

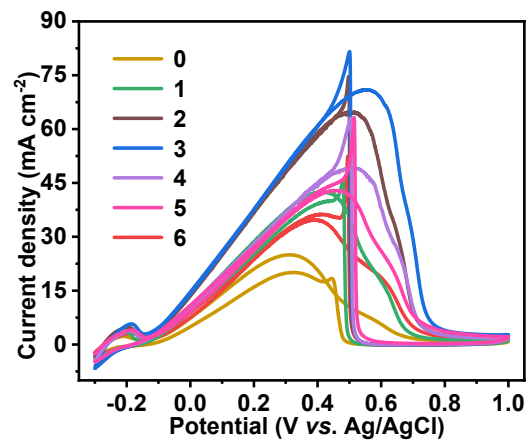


Figure S31. The comparison of FAO performance of the as-synthesized PdCuMoNiCo alloys on different carbon supports. The supports represented by the numbers from 0 to 6 are CNT, RGO-CNT, RGO₂-CNT, RGO₃-CNT, RGO₄-CNT, RGO₅-CNT, and RGO, respectively.

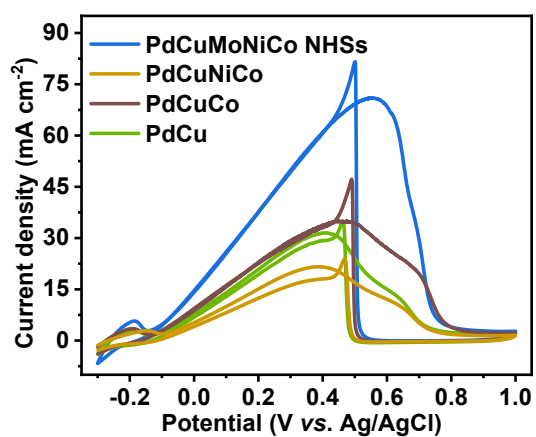


Figure S32. CV curves of the as-synthesized PdCu, PdCuCo, PdCuNiCo on RGO₃-CNT and PdCuMoNiCo NHSs/RGO₃-CNT recorded in Ar-saturated 0.1 M HClO₄ + 0.5 M HCOOH solution at a scan rate of 50 mV s⁻¹.

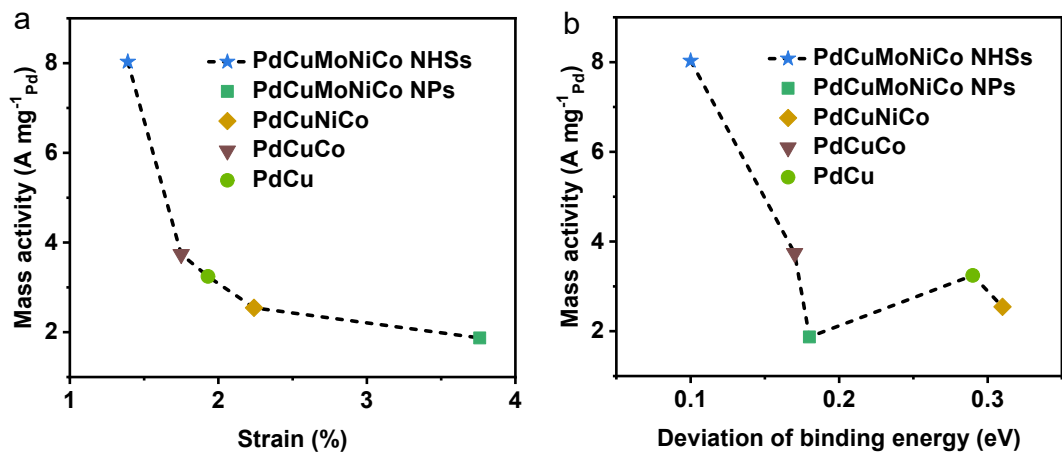


Figure S33. (a) The relationship between strain and MA of FAO. (b) The relationship between binding energy shift of Pd 3d XPS spectra and MA of FAO.

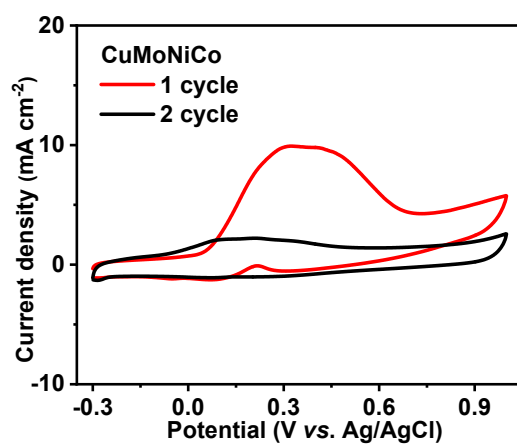


Figure S34. CV curves of CuMoNiCo on RGO₃-CNT in Ar-saturated 0.1 M HClO₄ + 0.5 M HCOOH solution at a scan rate of 50 mV s⁻¹.

Figure S34 demonstrates that the CuMoNiCo on RGO₃-CNT owns the poor catalytic activity of FAO, indicating that Pd is the active center in the PdCuMoNiCo NHSs/RGO₃-CNT toward FAO.

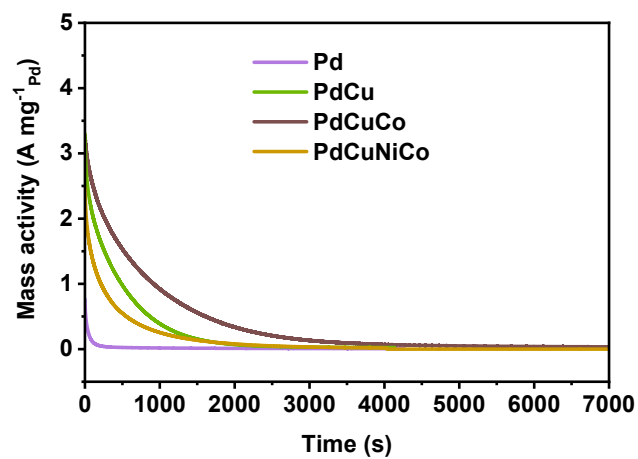


Figure S35. The current-time curves of the as-synthesized Pd, PdCu, PdCuCo, and PdCuNiCo on RGO₃-CNT for FAO at 0.5 V vs. RHE, respectively.

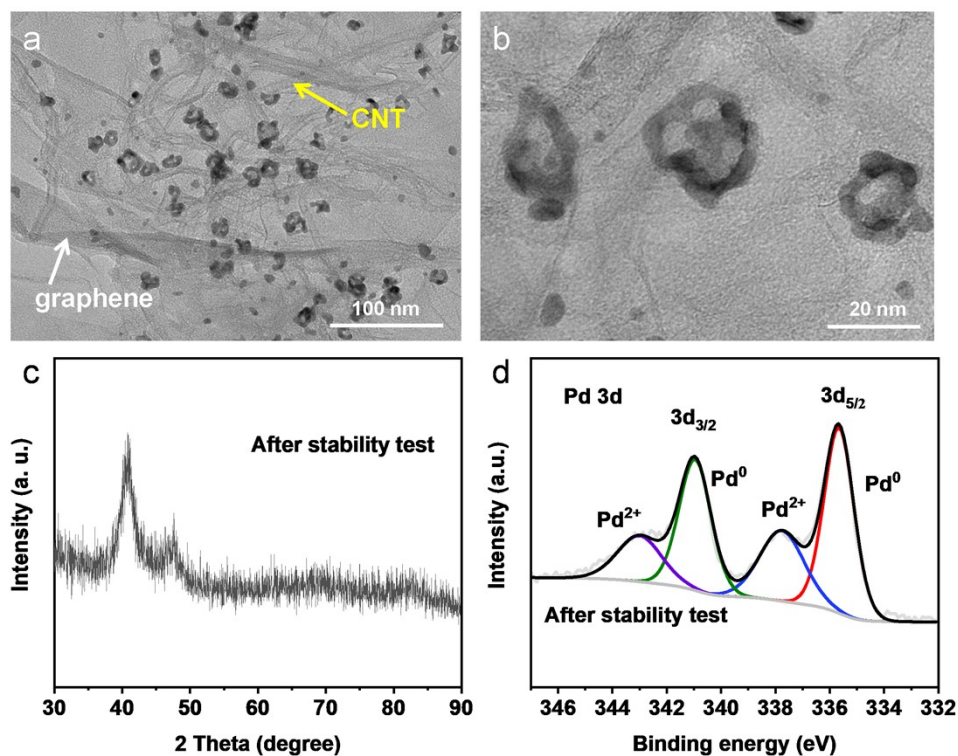


Figure S36. (a) TEM image, (b) HR-TEM image, (c) XRD pattern, and (d) High resolution of Pd 3d XPS spectrum of the PdCuMoNiCo NHSs/RGO₃-CNT after long-term durability test for FAO.

The morphology and size of nanohollow spheres in PdCuMoNiCo NHSs/RGO₃-CNT after the stability test are well maintained as shown in the TEM images (Figure S36a, b). The XRD pattern of the PdCuMoNiCo NHSs/RGO₃-CNT after the long-term durability test exhibits the characteristic peaks of the *fcc* Pd (Figure S36c), and matches well with the result before the stability test (Figure 3a). The main chemical state of Pd in the PdCuMoNiCo NHSs/RGO₃-CNT after the long-term durability test is the metallic state (Figure S36d), similar as that before the stability test (Figure 3c).

Table S1. The XRD results of different samples.

Samples	2θ / degree (111)	Lattice Parameter (nm)	Strain (%)
Pd	40.40	0.2232	--
PdCu NPs	42.61	0.2122	4.93
PdCu	41.25	0.2189	1.93
PdCuCo NPs	42.23	0.2140	4.12
PdCuCo	41.16	0.2193	1.75
PdCuNiCo NPs	42.09	0.2147	3.81
PdCuNiCo	41.41	0.2182	2.24
PdCuMoNiCo NPs	42.07	0.2148	3.76
PdCuMoNiCo NHSs	41.01	0.2201	1.39

Table S2. Element ratios of different samples detected by XPS.

Samples	Element	Atomic (%) (result from XPS)
Pd	Pd	100
PdCu	Pd	61
	Cu	39
PdCuCo	Pd	54
	Cu	32
	Co	14
PdCuNiCo	Pd	29
	Cu	16
	Ni	43
	Co	12
PdCuMoNiCo NPs	Pd	43
	Cu	21
	Mo	4
	Ni	15
	Co	17
	Pd	34
	Cu	16
PdCuMoNiCo NHSs	Mo	5
	Ni	28
	Co	17

Table S3. The deviation of binding energy of Pd 3d XPS spectra of different samples.

Samples	Deviation of binding energy (eV)
Pd	--
PdCu	0.29
PdCuCo	0.17
PdCuNiCo	0.31
PdCuMoNiCo NPs	0.18
PdCuMoNiCo NHSs	0.10

Table S4. Summary of MA of the different samples towards ORR and FAO.

Samples	ECSA (m² g⁻¹_{Pt or Pd})	MA for ORR (A mg⁻¹_{Pt or Pd})	MA for FAO (A mg⁻¹_{Pt or Pd})
Pt/C	32.7	0.007	0.781
Pd/C	75.5	0.630	0.231
Pd	61.0	0.092	1.016
PdCu	110.9	0.417	3.243
PdCuCo	98.5	0.421	3.741
PdCuNiCo	86.0	0.279	2.544
PdCuMoNiCo NPs	100.0	0.149	1.872
PdCuMoNiCo NHSs	142.0	0.882	8.030

Table S5. The ECSAs of different samples.

Samples	ECSA (m² g⁻¹_{Pd})
PdCu NPs	99.3
PdCu	110.9
PdCuCo NPs	76.8
PdCuCo	98.5
PdCuNiCo NPs	79.1
PdCuNiCo	86.0
PdCuMoNiCo NPs	100.0
PdCuMoNiCo NHSs	142.0

References

- [1] C. Hu, H. Cheng, Y. Zhao, Y. Hu, Y. Liu, L. Dai and L. Qu, *Adv. Mater.*, 2012, 24, 5493-5498.
- [2] L. Yang, C. Hu, J. Wang, Z. Yang, Y. Guo, Z. Bai and K. Wang, *Chem. Commun.*, 2011, 47, 8581-8583.